Astron. Astrophys. 322, 975–981 (1997)

ASTRONOMY AND ASTROPHYSICS

The chemical structure of bipolar planetary nebulae⋆

I. IC 4406

Romano L.M. Corradi[1], **Mario Perinotto**[2], **Hugo E. Schwarz**[3], **and Jean-François Claeskens**[4]

[1] Instituto de Astrofisica de Canarias, c. Via Lactea S/N, E-38200 La Laguna, Tenerife, Spain
[2] Dipartimento di Astronomia e Scienza dello Spazio, Università di Firenze, Largo E. Fermi 5, I-50125 Firenze, Italy
[3] Nordic Optical Telescope, Apartado 474, E-38700 Sta. Cruz de La Palma, Spain
[4] Institut d'Astrophysique, Université de Liège, 5 Avenue de Cointe, B-4000 Liège, Belgium

Received 14 May 1996 / Accepted 12 December 1996

Abstract. Long slit spectrophotometry of the bipolar planetary nebula IC 4406, in the range from 360 to 930 nm, has been used to study the chemical structure along its major axis. We find that:
– the He, O, N, Ne, and Ar abundances are constant, within errors, along the major axis of the nebula. Average values for He/H, O/H, N/H, Ne/H, and Ar/H are: 0.126, 5.6×10^{-4}, 2.0×10^{-4}, 1.7×10^{-4} and 3.2×10^{-6}, respectively. The N and He abundances of IC 4406 are quite modest for objects in this morphological class.
– The computed abundances of sulphur indicate an increase of S/H towards the external parts of the nebula, which may likely reflect inaccuracies in the available ionization correction factors.

Within the accuracy of the present data and analysis method, IC 4406 appears therefore to be a *chemically homogeneous* object.

Key words: ISM: abundances – planetary nebulae: individual: IC 4406

1. Introduction

Bipolar objects form a distinctive class of planetary nebulae (PNe). Here the term "bipolar" is used to indicate nebulae which consist of an equatorial waist from which two symmetrical lobes depart in the perpendicular directions, as opposed to elliptical PNe in which the central waist is absent (Schwarz et al. 1993). These nebulae are also referred to as "butterfly" in the literature (Balick 1987). Besides their characteristic morphology, bipolar PNe show a number of peculiar properties (see Corradi & Schwarz 1995 – hereafter CS95 – for a recent extensive analysis and for references to previous studies): they belong to a younger Galactic disc population than elliptical objects, have the hottest central stars among PNe, chemical overabundances of helium, nitrogen, and possibly neon, outflow velocities of up to one order of magnitude larger than the typical expansion velocities of PNe, large neutral envelopes, and peculiar IRAS colours. Some of the above properties indicate that bipolar PNe are produced by more massive progenitors than PNe of the other morphological classes.

Chemically, bipolar nebulae belong to the class of type I PNe (Peimbert & Torres-Peimbert 1983) defined by having either He/H $\gtrsim 0.125$ or log(N/O) $\gtrsim -0.3$. The most likely reason for this overabundance in He and/or N relative to the Sun and to most of the other PNe is that massive AGB stars ($M_i \gtrsim 2$ M$_\odot$) are expected be substantially He and/or N enriched at their surface, following second and third dredge-up episodes as well as a consequence of efficient H-burning at the base of the convective envelope (Renzini & Voli 1981). Modern calculations (Marigo et al. 1996) fail, however, to reproduce the He and N overabundances measured in several bipolar PNe, at least for the considered range of progenitor masses ($0.7 \leq M_i \leq 4$ M$_\odot$).

Although chemical abundances are available for many PNe, including bipolar PNe, these determinations are not all of the same accuracy (cf. Perinotto, 1991 for a critical compilation of abundances of galactic PNe). New, homogeneous, high quality chemical data are still needed to improve our knowledge on the subject. We have obtained deep long-slit spectra of about fifteen bipolar nebulae selected from the compilation of CS95. These data allow us to obtain an homogeneous set of chemical abundances for this morphological class of PNe, as well as to address the question of possible abundance variations inside the nebulae. This is an important topic, because material found at different positions in a PN could be the result of various mass loss episodes or trace the chemical inhomogeneities in the original mass outflow. In this paper, we discuss the results for the bipolar PN IC 4406, illustrating in detail observations, data reduction, and the analysis method. The results for the other nebulae will be presented in a forthcoming paper.

Send offprint requests to: R. Corradi (rcorradi@iac.es)

⋆ Based on observations made at the European Southern Observatory

2. IC 4406

IC 4406 (PN G319.6+15.7) is a large ($\sim$ 100″ long) southern bipolar PN. Optical CCD images of the nebula are presented by Sahai et al. (1991), Schwarz et al. (1992), and Corradi & Schwarz (1993). In these images, IC 4406 appears to be composed by two elongated lobes, mostly prominent in the light of low ionization species such as [NII]λ658.3, extending from a bright central region showing evidence for the presence of a large torus of ionized gas. CO observations (Sahai et al. 1991) indicate that the ionized gas is located inside a cylindrical molecular cavity; the CO expansion velocity increases from $\sim$ 15 km s^{-1} in the equatorial plane to 60-70 km s^{-1} along the polar directions of the cylinder. An optical velocity field of the nebula has been obtained by Corradi & Schwarz (1993), but velocities are not resolved there. In the central region, roughly corresponding to the equatorial ionized torus, shocked H_2 emission has been detected (Storey 1984), which is supposed to be produced at the interface between ionized and molecular gas (Sahai et al. 1991). The morphological and kinematical properties of IC 4406 indicate that the mass outflow has been collimated by an equatorial density enhancement in the circumstellar envelope ejected by the progenitor, in agreement with the current view of formation of bipolar PNe (Balick 1987).

The major axis of the nebula lies very close to the plane of the sky. Sahai et al. (1991) derived a nebular inclination (angle i between the symmetry axis of the nebula and the line of sight) of 78°.5±3°. This inclination makes IC 4406 an ideal target to look for chemical gradients, since every line of sight intersects regions of the nebula which are all approximately at the same distance from the centre. Mixing of emission coming from regions at different distances from the central star is therefore minimized.

Previous studies of the chemical abundances of IC 4406 have been presented by Kaler (1978, 1983), de Freitas Pacheco et al. (1992), and Perinotto et al. (1994), but they lack spatial resolution or are limited to the bright central part of the nebula.

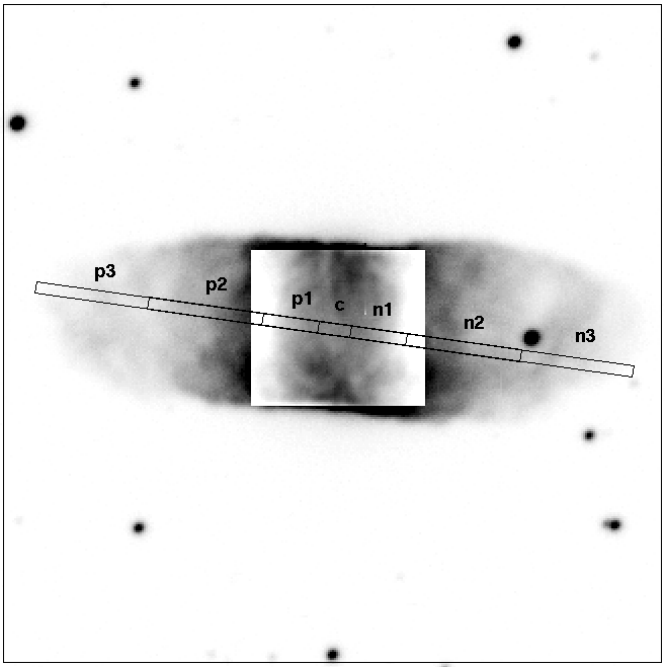

Fig. 1. The Hα+[NII]658.3 image of IC 4406 (from Corradi & Schwarz 1993). North is at the top, East to the left. The inset in the image is reproduced with different cuts to show up the bright inner nebula. The total field of view is 114″×114″. A drawing of the adopted slit position is superimposed on the image. In the slit we have indicated the seven regions from which average 1-D spectra were extracted (see text).

3. Observations and reduction

IC 4406 was observed on March 1994, at the 1.52m ESO telescope of La Silla, Chile, equipped with a Boller & Chivens spectrograph. The detector used was a Ford FA2048L CCD. On the first night, the ESO grating No.25 was used giving a reciprocal dispersion of 0.28 nm pix^{-1} (spectral resolution 2 pix) and a useful spectral range from 360 nm to 840 nm (see below). The slit of the spectrograph was placed on the long axis of the nebula and passed through its central star. The position angle (P.A.=+82°) was chosen as to avoid a foreground star which lies almost exactly along the symmetry axis of IC 4406. A drawing of the slit, superimposed on an Hα+[NII]658.3 image of the nebula taken from Corradi & Schwarz (1993), is shown in Fig. 1. The slit width was 2″, and the spatial scale along the slit 0″.82 pix^{-1}. With this configuration, two spectra with exposure times of 45 and 60 min were obtained. The seeing was around 1″.5 FWHM (full width at half maximum).

On the second night, red spectra of IC 4406 were obtained by using ESO grating No.14 and an order separator filter cutting all wavelengths below 680 nm. The useful spectral range is from 710 nm to 930 nm, with a reciprocal dispersion similar to that of the blue spectrum. Two exposures of 2 and 45 min were obtained. The slit width and position angle were the same as for the blue spectrum. Only in the central position the shorter exposure proved to be sufficiently exposed to allow to measure the line intensities and to compare them with the values given by the longer exposure. On each night, three spectrophotometric standard stars were also observed.

The data were reduced using the standard MIDAS procedure for long-slit spectroscopy. In the blue spectrum the instrumental response curves from individual standard stars agree within 10% of their mean value from 360 nm to 840 nm. This is the wavelength range that we have adopted for the subsequent analysis. Outside this range, the instrumental response curves from different standard stars deviate significantly (>20%). For similar reasons and because of uncertainties in the absolute fluxes tabulated for the selected standard stars above 950 nm, we have used a spectral range between 710 nm and 930 nm, although in the original spectrum nebular lines as red as the HeIλ1083 nm were detected.

Table 1. The selected regions of IC 4406

Region	Distance[1]	Size[2]
*p*3	+42.2	19.7
*p*2	+22.5	19.7
p1	+7.8	9.8
c	0	5.7
*n*1	−7.8	9.8
*n*2	−22.5	19.7
*n*3	−42.2	19.7

[1] Distance in arcsec of the middle point of the region from the centre of the nebula. The plus sign indicates positions in the eastern lobe, the minus in the western one.
[2] Size of the region in arcsec.

3.1. Flux measurements

Line emission from several ions was detected through the whole ($\sim$105″) optical extent of IC 4406. Before measuring line fluxes, one-dimensional spectra of a number of regions were extracted by spatial binning along the slit. We have decided to divide the section of IC 4406 covered by the slit into seven parts (a central region, plus three symmetrical ones on each side of the central star), in order to increase the S/N ratio in the faint lobes while keeping a good number of positions where to investigate for radial variations of chemical abundances. In the following the central region is referred to as *c*, while regions on the eastern lobe (the "positive" side of the nebula according to the oriented direction defined by P.A.=+82°) are named *p1*, *p*2, and *p*3 for increasing distances from the centre, respectively. Analogously, the three regions on the western ("negative") lobe are called *n*1, *n*2, and *n*3. The exact location of the middle point of each region and its extension are given in Table 1. The limits of the regions are also indicated in Fig. 1.

Line fluxes in the average 1-D spectra were measured using the MIDAS/ALICE package: multi-Gaussian analysis was performed to separate partially blended components. Line fluxes measured in the two spectra with different exposure times in the same position were then averaged with a weight proportional to the exposure time, after normalisation within each spectrum to Hβ. In the blue spectra, the errors on the average fluxes have been estimated by considering the deviations of the individual measurements from the average values. These deviations resulted larger than the errors as computed by the MIDAS/ALICE program from the r.m.s. of the continuum fit, and larger in the more external positions than in the positions closer to the central star. Accordingly, the errors on the average fluxes have been adopted as follows. In positions *n*2, *n*3, *p*2, *p*3, they are taken to be as large as 10%, 20%, 30% and 50% for the lines whose intensity is $>0.2\cdot$Hβ, between 0.05 and $0.2\cdot$Hβ, between 0.01 and $0.05\cdot$Hβ, and $<0.01\cdot$Hβ, respectively. It has to be mentioned than only in very few cases in the subsequent analysis we will use line whose intensity is less than 0.01 Hβ. For the central positions (*n*1, *c*, *p1*), which are significantly brighter, the estimated uncertainty of the average fluxes resulted to be

Table 2. Observed line fluxes.

Identification		*n*3	*n*2	*n*1	*c*	*p1*	*p*2	*p*3
372.70	[OII]	936.1	496.2	286.9	265.9	312.3	483.0	956.2
374.90	blend	–	2.7	–	–	3.0	–	–
377.06	H_{11}	–	3.0	2.4	–	2.4	2.3	–
379.79	H_{10}	–	3.5	3.1	2.8	3.1	3.7	–
381.96	HeI	–	–	0.5	–	–	–	–
383.54	H_9	–	5.4	5.3	5.4	5.5	5.5	–
386.87	[NeIII]	111.1	101.7	101.1	99.2	105.7	107.9	115.6
388.90	H_8	22.0	21.4	18.6	18.1	20.0	22.7	21.3
396.84	HeII	48.9	48.9	46.6	46.0	48.0	49.7	55.0
402.64	HeI	–	–	2.1	2.0	2.4	2.4	–
407.20	blend	–	–	2.6	2.3	2.5	3.5	–
410.18	Hδ	19.0	24.4	23.8	25.2	24.7	23.8	20.9
426.72	CII	–	–	–	0.8	0.6	–	–
434.05	Hγ	45.5	43.9	42.8	43.3	43.6	49.7	50.7
436.32	[OIII]	–	5.1	7.0	7.7	6.8	4.8	–
438.79	HeI	–	–	–	–	0.6	–	–
439.20	–	–	–	2.5	–	–	–	–
447.15	HeI	9.6	6.5	5.2	5.0	5.2	5.5	–
454.16	HeII	–	–	–	0.7	0.4	–	–
464.10	NIII	–	–	2.8	4.1	2.7	–	–
468.57	HeII	–	–	15.9	27.7	13.9	–	–
471.13	[ArIV]	–	–	2.1	3.2	1.9	–	–
474.02	[ArIV]	–	–	1.1	2.0	0.9	–	–
486.13	Hβ	100.0	100.0	100.0	100.0	100.0	100.0	100.0
492.19	HeI	–	2.6	1.9	0.9	1.8	2.5	–
495.89	[OIII]	160.1	315.7	–	371.1	371.0	323.7	172.8
500.68	[OIII]	471.5	948.6	1159.0	1135.2	1135.8	973.8	512.0
520.00	[NI]	26.3	7.8	5.2	4.8	5.4	7.3	23.0
541.15	HeII	–	–	1.4	2.4	1.1	–	–
551.77	[ClIII]	–	–	0.6	0.6	0.7	–	–
553.79	[ClIII]	–	–	0.5	0.4	0.5	–	–
575.46	[NII]	14.6	7.8	5.7	5.1	5.4	7.1	15.2
587.57	HeI	24.1	18.8	16.9	15.1	16.4	17.8	21.6
630.03	[OI]	104.9	36.5	29.9	26.9	26.7	31.8	96.2
631.21	[SIII]	–	–	–	–	–	1.1	–
636.38	[OI]	34.6	11.9	10.0	8.9	9.1	11.5	32.4
654.80	[NII]	353.5	182.5	132.7	120.1	126.3	179.6	341.0
656.28	Hα	331.6	325.1	344.7	342.7	328.4	321.4	338.1
658.34	[NII]	1045.8	541.4	390.6	356.9	376.0	533.6	1022.2
667.81	HeI	6.3	5.6	5.3	4.8	5.0	5.7	7.1
671.65	[SII]	117.5	29.2	8.9	5.8	8.9	31.2	114.7
673.08	[SII]	89.2	24.6	9.2	6.5	9.2	26.8	84.0
689.09	HeII	–	–	–	0.1	–	–	–
700.57	[ArV]	–	–	–	0.4	–	–	–
706.53	HeI	6.7	5.2	4.8	4.6	4.6	5.2	7.0
713.58	[ArIII]	31.4	32.6	33.6	31.9	32.0	33.4	32.9
717.75	HeII	–	–	–	0.5	–	–	–
723.75	[ArIV]	–	–	0.5	0.6	0.4	–	–
728.13	HeI	–	1.7	–	0.9	0.9	1.3	–
731.96	[OII]	–	8.3	8.2	8.0	7.7	8.0	–
733.02	[OII]	–	7.3	7.7	7.4	7.1	7.4	–
732.50	[OII]bl.	23.6	16.2	15.8	15.4	14.8	15.4	26.4
753.05	[ClIV]	–	–	–	0.2	–	–	–
759.27	HeII	–	–	–	0.4	–	–	–
775.11	[ArIII]	8.5	8.7	8.7	8.4	8.5	8.9	10.0
804.56	[ClIV]	–	–	0.3	0.4	0.3	–	–
819.65	CIII	–	–	–	0.4	–	–	–
823.68	HeII	–	–	0.5	1.2	0.5	–	–
841.33	–	–	–	–	0.3	–	–	–
843.80	–	–	–	–	0.4	–	–	–
846.73	–	–	–	–	0.4	–	–	–
850.25	P_{16}	–	–	0.5	0.5	0.5	–	–
854.54	P_{15}	–	–	0.7	0.7	0.7	–	–
857.87	–	–	–	0.5	0.5	0.5	–	–
859.84	P_{14}	–	–	0.9	0.9	0.9	–	–
866.50	P_{13}	–	–	1.4	1.4	1.3	–	–
872.71	[CI]	–	–	0.6	0.6	0.5	–	–
875.05	P_{12}	–	1.0	1.5	1.7	1.7	1.4	–
886.28	P_{11}	–	2.2	2.3	2.4	2.3	2.4	–
901.49	P_{10}	–	2.5	3.1	3.1	2.9	2.5	–
906.89	[SIII]	33.3	21.4	13.9	10.9	17.7	34.2	39.3
922.90	P_9	–	4.6	4.7	4.8	4.5	4.5	–
c_β		0.20	0.19	0.27	0.26	0.20	0.17	0.18
F(Hβ)*		0.32	1.65	4.16	3.38	4.42	1.50	0.23

*[10^{-13} erg cm^{-2} s^{-1}]

well represented by one half of the values quoted above. In the near-IR spectra, fluxes from the two differently exposed frames can be compared only in position *c*, and give deviations similar to those of blue spectra in the external positions. This spectral region, however, has larger uncertainties in the correction for the instrumental response curve, and we conservatively assign an error of 40% to the fluxes (note that only the [SIII]906.8 line is used in the following chemical analysis). Fluxes from the redder spectrum were then rescaled to the blue one using lines in the overlapping spectral region (710-840 nm). The average observed fluxes are listed in Table 2. Conditions during the observing run were photometric, and we also give in Table 2 the absolute flux of Hβ. We estimate the uncertainty on these absolute fluxes to be of the order of 30%.

4. Chemical analysis

4.1. Extinction, density and temperature

Fluxes have been de-reddened using the extinction law of Mathis (1990) with R_V=3.1. The logarithmic extinction constant c_β has been determined, in each of the selected regions, from the Balmer decrement in the relative averaged spectrum. They are listed in Table 2. At the centre, $c_\beta \sim 0.27$, in good agreement with previous optical and radio determinations (Torres-Peimbert & Peimbert 1977; Cahn et al. 1992; Tylenda et al. 1992).

The electron densities N_e have been computed from the [SII]673.1/671.7 intensity ratio, and electron temperatures from the [OIII] 495.9/436.3 and [NII] 658.3/575.5 ratios. The atomic data used throughout this paper are the same as in Kingsburgh & Barlow (1994, hereafter KB94). The computed density and temperature profiles of IC 4406 are shown in the upper panels of Fig. 2, and listed in Table 3 with their errors. At the centre, N_e=860 cm^{-3} decreasing in the outer parts to $\lesssim 100$ cm^{-3} (note that in *p*3 and *n*3 the [SII] ratio approaches its low density limit, where it is no longer sensitive to density variations). $T_{[NII]}$ and $T_{[OIII]}$ have a constant value, within errors, around $10000^\circ K$ throughout the nebula. In regions *n*3 and *p*3 the [OIII]λ436.3 line is not detected, and $T_{[OIII]}$ is assumed to be the same as in the neighbouring positions.

4.2. Chemical abundances

Given the temperatures and densities, the ionic abundances relative to hydrogen in each of the selected regions are computed from the line fluxes relative to Hβ. The concentration of He ions relative to hydrogen has been derived from the usual recombination lines assuming case B with the effective recombination coefficients from Hummer & Storey (1987) for HeII and Hβ lines and from Brocklehurst (1971) for the HeI lines. Corrections of the HeI lines for the effect of collisional population of their upper states via excitation from the 2^3S metastable level was evaluated using the prescriptions by Clegg (1987). Owing to the low densities, this contribution was found to be below 1-3 % and consequently no correction for the effect has been applied.

Errors on the ionic abundances from a single spectral line are derived by taking into account both the errors in the line ratios and those on the adopted temperature. To obtain the total abundances, the ionization correction factors (*icf*) from KB94 are used. Errors on the total abundances are obtained by propagating the errors on the mean ionic abundances as well as on the *icf*. Ionic and total abundances are listed in Table 4. Abundance profiles are shown in Fig. 2. We discuss the results for the different elements separately.

Helium. The He/H abundance is constant throughout the nebula around the value of 0.125 except for the extreme positions *n*3 and *p*3 where it apparently increases to $\sim$0.15. Owing to the to larger errors in the outer positions, we cannot conclude that the effect is real. A confirmation by further observations would be however in order, considering the important implications of such a result. The mean He/H abundances throughout the nebula, obtained by weighting the determinations in the different positions with both their errors and a "mass" factor (proportional to the square root of the total Hβ flux from that region), is 0.126$\pm$0.015.

Oxygen. We measure a substantial amount of O^0 particularly in the outer parts of the nebula. On the other hand, where O^0 is abundant, the same could be inferred of the neutral hydrogen. Excluding O^0 in the computation of the total O/H abundance, therefore, is to some extent compensated by the fact that also the neutral hydrogen is not taken into account. We have then derived the total O/H abundance by the formula O/H=$(O^+/H^+ + O^{2+}/H^+)\cdot$*icf*, as done by KB94, where *icf*(O) accounts for the contribution of the ionization stages higher than O^{2+}. In this way, the total oxygen abundance results to be constant throughout IC 4406, with an average value of is 5.60$\pm$1.26 ($\times 10^{-4}$).

Nitrogen. Similarly to oxygen, the N/H total abundance is constant throughout the nebula. The weighted mean of N/H is 2.01$\pm$0.87 ($\times 10^{-4}$), and the average $\log N^+/O^+ \cong \log N/O = -0.43$ (which is constant within 8% throughout the seven positions). Both are quite modest values for bipolar PNe (CS95).

Neon, argon and sulphur. The situation for these elements is less clear. While the ionic abundances do not show dramatic variations along the nebulae, when *icf* are applied a significant increase of the total abundances toward the external regions appears. The effect, although systematic in the three elements, remains within the estimated errors for Ne and Ar, while it is larger than the errors for sulphur. Note that the sum of the argon abundances in three different ionic stages (Ar^{2+}+Ar^{3+}+Ar^{4+}) is on the other hand pretty constant. We then suspect that the used *icf*, in particular for sulphur, do not correctly describe the ionization structure of the nebula. The weighted means of Ne/H and Ar/H are 1.68$\pm$0.70 ($\times 10^{-4}$) and 3.19$\pm$1.12 ($\times 10^{-6}$), respectively.

5. Discussion and conclusions

IC 4406 just meets the condition for Type I PNe of having He/H $\gtrsim$ 0.125. On the other hand, its N/O abundance ratio is not strongly enhanced. According to its morphology (the equa-

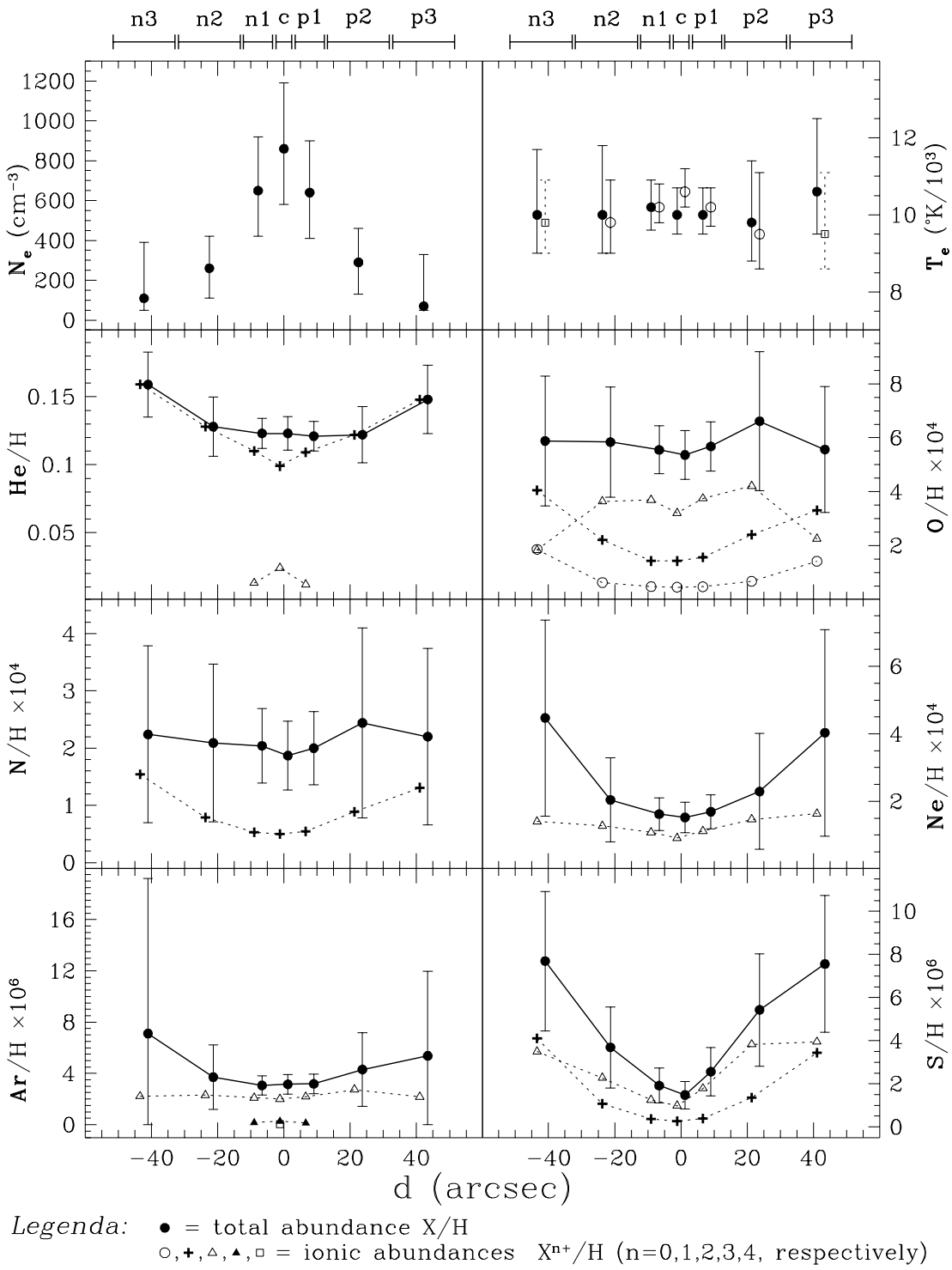

Fig. 2. Density, temperature, and abundance profiles for IC 4406. $T_{[NII]}$ and $T_{[OIII]}$ are indicated by filled and open circles, respectively (open squares are *adopted* $T_{[OIII]}$). Symbols are plotted slightly displaced in d in order to avoid overlapping. In the lower panels, ionic and total abundance profiles for He, O, N, Ne, Ar, and S are shown. The explanation of the symbols used is given in the *Legenda* at the bottom of the figure. Above the uppermost boxes, the limits of the regions into which the slit was divided are indicated by horizontal "errorbars".

Table 3. Electron density and temperature in IC 4406. In brackets are *adopted* temperatures.

		*n*3	*n*2	*n*1	*c*	*p1*	*p*2	*p*3
N_e	(cm^{-3})	110^{+280}_{-110}	260^{+160}_{-150}	650^{+270}_{-230}	860^{+330}_{-280}	640^{+260}_{-230}	290^{+170}_{-160}	70^{+260}_{-70}
$T_{[OIII]}$	(°K)	(9800^{+1100}_{-800})	9800^{+1100}_{-800}	10200^{+600}_{-400}	10600^{+600}_{-400}	10200^{+500}_{-500}	9500^{+1600}_{-900}	(9500^{+1600}_{-900})
$T_{[NII]}$	(°K)	10000^{+1700}_{-1000}	10000^{+1800}_{-1000}	10200^{+700}_{-600}	10000^{+700}_{-500}	10000^{+700}_{-500}	9800^{+1600}_{-1000}	10600^{+1900}_{-900}

Table 4. Chemical abundances of IC 4406. In brackets are the % errors on the total abundances.

Ion/Elem.	line	*n*3	*n*2	*n*1	*c*	*p1*	*p*2	*p*3
He^+/H	4471	0.204	0.137	0.114	0.105	0.110	0.113	–
	5876	0.157	0.124	0.106	0.095	0.106	0.122	0.145
	6678	0.141	0.124	0.110	0.102	0.110	0.134	0.156
	mean	0.159	0.128	0.110	0.099	0.109	0.122	0.148
He^{2+}/H	4686	–	–	0.013	0.024	0.012	–	–
He/H	total	0.159 (15)	0.128 (17)	0.123 (9)	0.123 (10)	0.121 (9)	0.122 (17)	0.148 (17)
$O^0/H \times 10^4$	6300	1.83	0.63	0.47	0.45	0.46	0.64	1.40
	6364	1.89	0.64	0.49	0.46	0.49	0.72	1.45
	mean	1.86	0.63	0.48	0.46	0.47	0.68	1.42
$O^+/H \times 10^4$	3727	4.09	2.13	1.35	1.35	1.47	2.26	3.20
	7325	3.95	2.39	1.70	1.68	1.83	2.91	3.61
	mean	4.05	2.21	1.43	1.43	1.56	2.40	3.31
$O^{2+}/H \times 10^4$	4959	1.82	3.57	3.61	3.13	3.65	4.13	2.22
	5007	1.85	3.71	3.80	3.30	3.86	4.30	2.28
	mean	1.84	3.64	3.70	3.21	3.75	4.21	2.25
icf		1.00	1.00	1.08	1.15	1.07	1.00	1.00
O/H $\times 10^4$	total	5.88 (41)	5.84 (35)	5.55 (16)	5.36 (17)	5.68 (16)	6.61 (39)	5.56 (42)
$N^+/H \times 10^5$	6548	15.40	7.86	5.29	5.00	5.46	8.83	13.30
	6583	15.40	7.89	5.27	5.03	5.48	8.90	13.20
	mean	15.40	7.87	5.28	5.02	5.47	8.86	13.10
icf		1.45	2.64	3.86	3.72	3.64	2.75	1.68
N/H $\times 10^4$	total	2.24 (69)	2.09 (66)	2.04 (32)	1.87 (32)	2.00 (32)	2.44 (68)	2.20 (70)
$Ne^{2+}/H \times 10^4$	3869	1.40	1.27	1.08	0.91	1.12	1.46	1.63
icf		3.20	1.61	1.50	1.67	1.52	1.57	2.47
Ne/H $\times 10^4$	total	4.47 (65)	2.04 (61)	1.62 (30)	1.52 (30)	1.69 (30)	2.29 (75)	4.03 (76)
$Ar^{2+}/H \times 10^6$	7135	2.22	2.31	2.10	2.00	2.19	2.74	2.17
$Ar^{3+}/H \times 10^6$	4740	–	–	0.17	0.28	0.13	–	–
$Ar^{4+}/H \times 10^6$	7005	–	–	–	0.03	–	–	–
icf		3.20	1.61	1.35	1.37	1.38	1.57	2.47
Ar/H $\times 10^6$	total	7.11 (170)	3.71 (68)	3.06 (24)	3.15 (24)	3.19 (24)	4.30 (67)	5.37 (123)
$S^+/H \times 10^6$	6717	4.11	1.09	0.36	0.27	0.39	1.36	3.44
	6731	4.10	1.09	0.36	0.27	0.39	1.36	3.44
	mean	4.11	1.08	0.36	0.27	0.39	1.36	3.44
$S^{2+}/H \times 10^6$	6312	–	–	–	–	–	2.63	–
	9069	3.50	2.28	1.25	0.98	1.79	4.28	3.95
	mean	3.50	2.28	1.25	0.98	1.79	3.83	3.95
icf		1.01	1.10	1.19	1.18	1.17	1.12	1.02
S/H $\times 10^6$	total	7.69 (42)	3.69 (51)	1.92 (42)	1.48 (43)	2.56 (44)	5.43 (48)	7.56 (42)

torial waist is not very pronounced), kinematics (the polar expansion velocities are not very high), and chemistry (the He and N/O enrichment is modest), IC 4406 appears therefore to be a "moderate" bipolar PN.

Apart from the sulphur abundances, whose interpretation remains difficult, the results of the present study make IC 4406 a *chemically homogeneous* object. This is consistent with the idea that the nebula is the result of a single envelope ejection from the progenitor star, its elongated shape being the result of collimation processes in the chemically homogeneous, coeval ejecta.

Our abundance determinations can be compared with those from previous studies of IC 4406, at least for its central region. de Freitas Pacheco et al. (1992) found He/H=0.095, substan-

tially lower than the values of 0.141 (Kaler 1978, 1983), 0.13-0.14 (Perinotto et al. 1994), and 0.126 (present work). Significant differences between de Freitas Pacheco et al. (1992) and our work are also found for oxygen, nitrogen, and argon, whose abundances are by a factor $\gtrsim 1.5$ higher in their study. Our abundances show better agreement with those of Kaler (1978, 1983) and Perinotto et al. (1994), although variations of up to 30% are the rule rather than the exception. These numbers give an idea of the actual uncertainty in the PNe abundances available in the literature.

Another point to be considered in the future, when a better understanding of the problem will be reached, is the question of whether the ionic abundances derived by the intense collisionally excited forbidden lines are really accurate. Recent studies (e.g. Liu et al., 1995) have in fact shown that there is a clear discrepancy between the chemical abundances for heavy ions (in particular O^+) computed by collisionally excited lines and those from recombination lines, the latter ones being up to a factor of five higher. A full explanation of this discrepancy is not available yet, even taking into account the temperature fluctuations scheme of Peimbert (1967).

To our knowledge, the only other chemical studies of bipolar PNe with detailed spatial information are those by Guerrero (1995) on NGC 2440 and NGC 2818, and by Guerrero et al. (1996) on K 4-55. NGC 2818 appears to be similar to IC 4406 in showing constant abundances along its major axis. On the contrary, significant chemical variations are found in the various morphological components of NGC 2440 and K 4-55, which are interpreted as due to successive mass loss episodes of newly enriched material from their progenitors. These very different results illustrate the interest in pursuing this kind of spatially detailed chemical studies of bipolar PNe.

Acknowledgements. The work of RLMC has been supported by a grant of the "Human Capital and Mobility Programme" of the European Community. We are grateful to M.J. Barlow for providing information on his list of recent atomic data, and M. Guerrero for useful discussion on the topics presented in this paper.

References

Balick, B: 1987, AJ 94, 671
Brocklehurst, M. : 1971, MNRAS 153, 471
Cahn, J.K., Kaler, J.B., Stanghellini, L.: 1992, A&AS 94, 399
Clegg, R.E.S. : 1987, MNRAS 229, 31p
Corradi, R.L.M., Schwarz, H.E.: 1993, A&A 278, 247
Corradi, R.L.M., Schwarz, H.E.: 1995, A&A 293, 871 (**CS95**)
de Freitas Pacheco, J.A., Maciel, W.J., Costa, R.D.D.: 1992, A&A 261, 579
Guerrero, M.A.: 1995, Thesis, University of La Laguna, Tenerife, Spain
Guerrero, M.A., Manchado, A., Serra-Ricart, M.: 1996, ApJ 456, 651
Hummer, D.G., Storey, P.J.: 1987, MNRAS 224, 801
Kaler, J.B.: 1978, ApJ 225, 527
Kaler, J.B.: 1983, in Planetary nebulae, IAU Symp.n.103, Flower ed., p.557
Kingsburgh, R.L., Barlow, M.J.: 1994, MNRAS 271, 257 (**KB94**)
Liu, X.-W., Storey, P.J., Barlow, M.J., Clegg, R.E.S.: 1995, MNRAS 272, 369
Marigo, P., Bressan, A., Chiosi, C.: 1996, A&A, in the press
Mathis, J.S.: 1990, ARA&A 28, 37
Peimbert, M.: 1967, ApJ 150, 825
Peimbert, M., Torres-Peimbert, S.: 1983, in Planetary nebulae, IAU Symp.n.103, Flower ed., p.233
Perinotto, M. : 1991, ApJS 76, 687
Perinotto, M., Purgathofer, A., Pasquali, A., Patriarchi, P.: 1994, A&AS 107, 481
Renzini, A., Voli, M.: 1981, A&A 94, 175
Sahai, R., Wootten, A., Schwarz, H.E., Clegg, R.E.S.: 1991, A&A 251, 560
Schwarz, H.E., Corradi, R.L.M., Melnick, J.: 1992, A&AS 96, 23
Schwarz, H.E., Corradi, R.L.M., Stanghellini, L.: 1993, in Planetary nebulae, IAU Symp. N.155, eds. Weinberger & Acker, p. 214
Storey, J.W.V.: 1984, MNRAS 206, 521
Tylenda, R., Acker, A., Stenholm, B., Koppen, J.: 1992, A&AS 95, 337
Torres-Peimbert, S., Peimbert, M.: 1977, Rev. Mex. Astron. Astrof. 2, 181

This article was processed by the author using Springer-Verlag LaTeX A&A style file *L-AA* version 3.